Linking hydrothermal deactivation of Cu-CHA catalysts for NH3-SCR to dealumination and reduced [Cu2(NH3)4O2]2+ formation

Downloaded from: https://research.chalmers.se, 2026-11-07 10:38 UTC

Citation for the original published paper (version of record):
Singh, S., Janssens, T., Grönbeck, H. (2026). Linking hydrothermal deactivation of Cu-CHA catalysts for NH3-SCR to dealumination and reduced [Cu2(NH3)4O2]2+ formation. Catalysis Science and Technology, 16(8): 2889-2898. http://dx.doi.org/10.1039/d5cy01491c

N.B. When citing this work, cite the original published paper.

research.chalmers.se offers the possibility of retrieving research publications produced at Chalmers University of Technology. It covers all kind of research output: articles, dissertations, conference papers, reports etc. since 2004. research.chalmers.se is administrated and maintained by Chalmers Library

(article starts on next page)

Catalysis Science & Technology

ROYAL SOCIETY OF CHEMISTRY

PAPER

View Article Online
View Journal | View Issue

Check for updates

Cite this: *Catal. Sci. Technol.*, 2026, **16**, 2889

Linking hydrothermal deactivation of Cu-CHA catalysts for NH_3-SCR to dealumination and reduced $[Cu_2(NH_3)_4O_2]^{2+}$ formation

Shivangi Singh,*[ab] Ton V. W. Janssens [c] and Henrik Grönbeck *[b]

Received 7th December 2025,
Accepted 5th March 2026

DOI: 10.1039/d5cy01491c

rsc.li/catalysis

NH_3-Selective Catalytic Reduction (NH_3-SCR) is a critical technology for controlling NO_x emissions from diesel and H_2 engines. Cu-exchanged chabazite (Cu-CHA) materials are preferred catalysts for the NH_3-SCR reaction thanks to high activity, selectivity and stability under normal operating conditions. However, exposure of Cu-CHA to water at high temperatures (≥650 °C) leads to loss of Brønsted acid sites due to dealumination. Here, we have measured the activity and selectivity of hydrothermally aged Cu-CHA. The hydrothermal deactivation is linked to changes in the amount of Brønsted acid sites as measured by NH_3-Temperature-Programmed Desorption (TPD) and the ability to form the key intermediate $[Cu_2(NH_3)_4O_2]^{2+}$, as probed by NO-Temperature-Programmed Reaction (TP Reaction). The activity decreases rapidly during the first 10 hours of aging, which correlates with a rapid loss of Brønsted acid sites. The activity after 10 hours is reduced at a slower rate, which coincides with a loss in ability to form $[Cu_2(NH_3)_4O_2]^{2+}$. The measurements are corroborated by density functional theory based microkinetic modeling. The simulations show that the part of the reaction cycle that occurs over Brønsted acid sites in fresh catalysts can occur at a slower rate over silanol nests in the aged catalyst. Roughly half of the activity loss after 100 hours of aging can be attributed to the decrease of Brønsted acid sites, whereas the remaining loss can be related to reduced formation of the $[Cu_2(NH_3)_4O_2]^{2+}$ complex.

Open Access Article. Published on 06 March 2026. Downloaded on 5/11/2026 12:46:31 PM.
This article is licensed under a Creative Commons Attribution 3.0 Unported Licence.

Introduction

Selective catalytic reduction of NO_x using ammonia as a reducing agent (NH_3-SCR) is the leading technology for controlling NO_x emissions in oxygen excess, such as diesel exhausts.[1,2] Cu-exchanged small-pore chabazite zeolites have shown high activity for NH_3-SCR and a good hydrothermal stability under low-temperature conditions.[1,3,4] The overall NH_3-SCR reaction with only NO (so-called standard SCR) is:

$$4NH_3 + 4NO + O_2 \rightarrow 4N_2 + 6H_2O$$

Each NO reacts with one NH_3 molecule, and O_2 is needed to accommodate the hydrogen atoms. The NH_3-SCR reaction cycle over Cu-CHA involves alternating oxidation and reduction of Cu ions, with the Cu oxidation state cycling between Cu^+ and Cu^{2+}. O_2 adsorption occurs on Cu^+ sites, oxidizing them to Cu^{2+}, whereas the coupling of NO and NH_3 reduces Cu^{2+} back to Cu^+.

Atomistic reaction mechanisms have been developed based on experiments and first principles calculations.[5–13] The reaction mechanisms agree that Cu-sites are required for the oxidation half cycle, whereas different paths have been suggested for N–N coupling and N_2 formation. The mechanisms include steps where N_2 is formed from NH_4NO_2 or H_2NNO decomposition partly *via* HONO as an intermediate. NH_4NO_2 and H_2NNO decomposition is generally assumed to be facile, and in ref. 12 it is proposed to occur over Brønsted acid sites.

We have previously proposed a detailed reaction scheme based on density functional theory (DFT) calculations and DFT-based microkinetic modeling.[5–7] Fig. 1 shows a simplified version of the proposed reaction mechanism for standard NH_3-SCR. Below 300 °C, NH_3 solvates the Cu ions, forming mobile $[Cu(NH_3)_2]^+$ complexes.[14–17] Pairs of the $[Cu(NH_3)_2]^+$ complexes (A) are needed to allow for adsorption and activation of O_2 *via* the formation of a $[Cu_2(NH_3)_4O_2]^{2+}$ peroxo complex (B), which is a key intermediate in the reaction cycle.[18–20] The reaction proceeds *via* adsorption of NO, which reacts with NH_3 to form H_2NNO and $[Cu_2(NH_3)_4OOH]^{2+}$ (C). H_2NNO can diffuse away from the Cu sites and decompose over Brønsted acid sites to produce N_2 and H_2O.[6,21] Another H_2NNO and an HONO molecule can form over $[Cu_2(NH_3)_4OOH]^{2+}$ giving $[Cu_2(NH_3)_4OH]^{2+}$ (D), over which a

[a] *Umicore Denmark ApS, DK-2970 Horsholm, Denmark*
[b] *Department of Physics and Competence Centre for Catalysis, Chalmers University of Technology, SE-412 96 Göteborg, Sweden. E-mail: shivangi.singh@chalmers.se, ghj@chalmers.se*
[c] *c/o Umicore AG & Co. KG, Rodenbacher Chaussee 4, 63457 Hanau, Germany*

Open Access Article. Published on 06 March 2026. Downloaded on 5/11/2026 12:46:31 PM.
This article is licensed under a Creative Commons Attribution 3.0 Unported Licence.

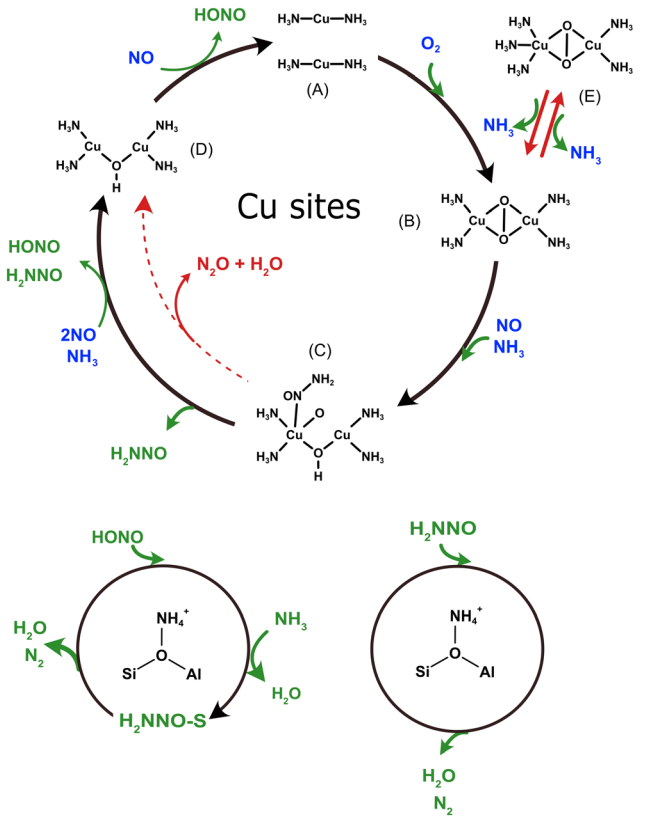

Fig. 1 Simplified reaction cycle for low-temperature NH_3-SCR over Cu-CHA, showing the most critical intermediates. The top cycle shows the formation of H_2NNO and HONO over Cu-sites, whereas the bottom cycles show the decomposition of H_2NNO and HONO over Brønsted acid sites. The kinetic simulations in the present work are performed with the complete low-temperature reaction cycle.[5–7]

second HONO molecule can form. Each HONO formed in the main reaction cycle decompose together with NH_3 over Brønsted acid sites to N_2 and H_2O. The Brønsted acid sites under reaction conditions are occupied by NH_3 forming NH_4^+, and thus H_2NNO and HONO are effectively decomposed over NH_4^+. An unwanted side reaction is N_2O formation, which may occur if H_2NNO decomposes over $[Cu_2(NH_3)_4OOH]^{2+}$.[22] The selectivity of the reaction depends critically on the ratio between the barriers for H_2NNO decomposition and diffusion together with the availability of Brønsted acid sites.[6] Adsorption of NH_3 competes with NO adsorption,[6] and results in $[Cu_2(NH_3)_5O_2]^{2+}$ (E). NH_3 adsorption blocks the Cu-sites for the reaction and $[Cu_2(NH_3)_5O_2]^{2+}$ is an inactive state of the catalyst, giving rise to the negative reaction order of the NH_3-SCR reaction in ammonia.[6] The proposed NH_3-SCR mechanism relies on both copper and Brønsted acid sites: HONO and H_2NNO form over copper sites and decompose over Brønsted acid sites.

Despite high activity and selectivity under low-temperature conditions, Cu-CHA catalysts are known to deactivate when exposed to water vapor at temperatures above 600 °C. This deactivation is a consequence of dealumination, and thus the detachment of Al^{3+} from the framework in the form of $Al(OH)_3H_2O$, so-called extra-framework Al (EFAl) species. In the dealumination process, four Si–OH groups (a silanol nest) are formed at the original locations of the Al^{3+} ions along with loss of a Brønsted acid site.[23–26] Furthermore, under high-temperature conditions, the loss of Brønsted acid sites may also be associated with the transformation of ZCuOH species into Z_2Cu.[27,28] X-ray absorption near edge spectroscopy (XANES) measurements show that the amount of $[Cu(NH_3)_2]^+$ complexes decreases upon dealumination.[29] The loss of $[Cu(NH_3)_2]^+$ complexes is accompanied by the formation of copper aluminate (Cu–Al) species, which are inactive for the NH_3-SCR reaction.[30] The Cu–Al species are formed by the reaction between Cu ions and extra-framework Al,[31] which according to our previous study is a thermodynamically preferred process.[32]

Dealumination and transformation of ZCuOH to Z_2Cu could affect the NH_3-SCR reaction rate both *via* the loss of Brønsted acid sites and changes in the properties of Cu-species.[33] If the decomposition of the HONO and H_2NNO intermediates to N_2 and H_2O occurs over Brønsted acid sites as proposed in Fig. 1, the loss of Brønsted sites should affect these reaction steps. Moreover, the distribution of Brønsted acid sites, which is changed upon dealumination, affects the mobility of the $[Cu(NH_3)_2]^+$ complexes and the stability of $[Cu(NH_3)_2]^+$ pairs[34,35] and the $[Cu_2(NH_3)_4O_2]^{2+}$ intermediate.[36]

In the present work, we link the loss in NH_3-SCR activity of Cu-CHA upon hydrothermal aging with changes in Brønsted acid sites and Cu sites. Activity measurements are combined with temperature-programmed desorption of NH_3 (NH_3-TPD), which measures the number of Brønsted acid sites, and NO-temperature-programmed reaction (NO-TP reaction), which estimates the amount of $[Cu_2(NH_3)_4O_2]^{2+}$ complexes. The activity as a function of aging time shows a rapid initial decrease followed by a slower decrease. We relate the rapid decrease to the loss of Brønsted acid sites, whereas the slow decrease is related to a reduced formation of $[Cu_2(NH_3)_4O_2]^{2+}$ complexes. The experiments are corroborated with density functional theory (DFT) calculations and DFT-based microkinetic modeling. The DFT calculations show that the barriers for HONO and H_2NNO decomposition over silanol sites are higher than those over Brønsted acid sites. The kinetic simulations suggest that approximately half of the reduced activity after 100 hours of aging is connected to the loss of Brønsted acid sites, whereas the rest of the activity loss can be attributed to reduced formation of $[Cu_2(NH_3)_4O_2]^{2+}$.

Experimental and computational details

Aging protocol

The experiments were performed with a Cu-CHA catalyst having a silica-to-alumina ratio (SAR) of 13.4, corresponding to a Si/Al ratio of 6.7, loaded with 3.2 wt% Cu. Cu-CHA is prepared by impregnation of the parent H-CHA material with

 This journal is © The Royal Society of Chemistry 2026

Open Access Article. Published on 06 March 2026. Downloaded on 5/11/2026 12:46:31 PM. This article is licensed under a Creative Commons Attribution 3.0 Unported Licence.

an appropriate amount of Cu-nitrate solution, followed by calcination at 600 °C for 2 h.

A catalyst portion of 50 mg was filled in a quartz U-tube microreactor with an inner diameter of 6 mm, and the initial activity and NH_3-TPD were measured. The fresh catalysts were pretreated by heating 10% O_2 at 550 °C. Hydrothermal aging was performed by exposing the catalyst to 10% water and 10% O_2 at 650 °C. The catalyst was subjected to stepwise hydrothermal aging to accumulate 1, 2, 5, 8, 10, 20, 40, 60, 80 and 100 hours of aging. After each step, the activity and NH_3-TPD were measured to follow the deactivation with the accumulated aging time. The amount of $[Cu_2(NH_3)_4O_2]^{2+}$ in the fresh and aged catalysts was measured in a separate measurement, after 2, 10 and 100 hours of accumulated aging. The parent H-CHA material was also used for some reference measurements.

Activity and selectivity measurements

For the fresh and aged catalysts, activity measurements were performed using 50 mg of dry catalyst material. The catalyst was exposed to a gas mixture containing 500 ppm NO, 600 ppm NH_3, 10% O_2, and 5% H_2O. The measurements were conducted at 160 °C in an N_2 carrier gas with a total flow rate of 13.5 NL h^{-1}. The concentrations of NO, NO_2, and N_2O were monitored using a Gasmet CX4000 FTIR spectrometer.

For the kinetic analysis, we used the common approximation that the NH_3-SCR reaction is first order in NO and zeroth order in NH_3.[37–39] The rate constant k (mol g^{-1} h^{-1}) is under these assumptions evaluated as:

$$k = -\frac{F \ln(1 - X_{NO})}{W} \quad (1)$$

where, F is the total molar flow (0.6027 mol h^{-1}), X_{NO} is the NO conversion, and W is the amount of catalyst (50 mg).

NH_3-temperature programmed desorption

To determine the effect of hydrothermal aging on the amount of Brønsted acid sites, we conducted NH_3-TPD measurements on the fresh catalyst samples and after hydrothermal aging at 650 °C in 10% O_2 and 10% H_2O for 1, 2, 5, 8, 10, 15, 20, 40, 60, 80, and 100 hours. For each experiment, a 50 mg sample (150–300 μm sieve fraction) mixed with 300 mg of SiC (mesh 60) was added to the quartz U-tube reactor.

The TPD measurement began with pre-heating the sample to remove any adsorbed species or moisture. Next, at 100 °C, the sample was exposed to 1500 ppm NH_3, followed by exposure to 5% water for 15 min to remove physisorbed NH_3, and an additional 60 min in dry N_2. Then, the catalyst was cooled to 80 °C, to start the heating ramp to 550 °C, at a rate of 3 °C min^{-1}.

NO temperature-programmed reaction

NO temperature-programmed reaction measurements was used to probe the amount of $[Cu_2(NH_3)_4O_2]^{2+}$ species formed in the catalyst.[40] The measurements were performed on a 50 mg sample aged at 650 °C for 0, 2, 10, and 100 hours. Prior to the measurements, the sample was heated at 550 °C with 10% O_2. The pretreatment was followed by cooling the sample to 200 °C, where it was exposed to 800 ppm NO and 960 ppm NH_3, which results in $[Cu(NH_3)_2]^+$ complexes.[41] Subsequent oxidation at 200 °C in 10% O_2 yields $[Cu_2(NH_3)_4O_2]^{2+}$ complexes.[41,42] After the oxidation, the samples were cooled to 50 °C, and exposed to 680 ppm NO while heating from 50 to 300 °C at a rate of 3 °C min^{-1}. During heating, we monitored the consumption of NO, from which the amount of $[Cu_2(NH_3)_4O_2]^{2+}$ was estimated.[40]

DFT calculations

Spin-polarized DFT calculations were performed using the Vienna *Ab initio* Simulation Package (VASP).[43–46] A plane wave basis set with a cutoff energy of 480 eV was used to describe the valence electrons. The interaction between the valence and the core electrons was described with the projector augmented wave (PAW) method.[47,48] The explicitly treated valence electrons were Si(4), Al(3), O(6), N(5), and H(1). The k-point sampling was restricted to the gamma point.

The Perdew–Burke–Ernzerhof PBE functional[49] augmented with D3 corrections to account for long-range van der Waals (vdW) interactions[50,51] was used to describe exchange correlation effects. The electronic structure was considered to be converged when the difference between steps in the Self-Consistent Field loop was smaller than 1×10^{-5} eV. Structures were considered to be relaxed when the force acting on each atom was smaller than 0.05 eV $Å^{-1}$.

The chabazite structure was modeled with a hexagonal unit cell, which includes 36 tetrahedrally coordinated silicon atoms (T-sites) in which one Si atom is substituted by an Al atom. Thus, the Si/Al ratio of the pristine zeolite is 35. Calculations are performed with the experimental lattice parameters of $a = b = 13.8$ Å, $c = 15.0$ Å, $\alpha = \beta = 90.0°$, and $\gamma = 120.0°$.

Mean-field microkinetic model

Mean-field microkinetic modeling was used to explore the consequences of replacing framework Al with silanol groups and facilitate comparison to experiments. Building on our previous work,[6,7] the present model replaces the Brønsted acid site with silanol groups as the active site for HONO and H_2NNO decomposition. The steady-state reaction rates and fractional intermediate concentrations were obtained by solving a set of coupled ordinary differential equations:

$$\frac{d\theta_i}{dt} = \sum_j c_{ji} r_j\left(\vec{\theta}\right) \quad (2)$$

where each intermediate i has a fractional concentration θ_i. r_j is the elementary reaction rates that depend on the fractional concentration of the intermediates ($\vec{\theta}$). c_{ji} is the stoichiometric factor of compound i in reaction j. The rate constant (k_j) for the reaction j is given by:[52]

Open Access Article. Published on 06 March 2026. Downloaded on 5/11/2026 12:46:31 PM.
This article is licensed under a Creative Commons Attribution 3.0 Unported Licence.

$$k_j = \frac{k_B T}{h} e^{-\Delta H^{\ddagger}/k_B T} e^{\Delta S^{\ddagger}/k_B} \approx \frac{k_B T}{h} e^{-\Delta E^{\ddagger}/k_B T} e^{\Delta S^{\ddagger}/k_B} \quad (3)$$

where k_B is Boltzmann's constant, T is the temperature, and h is Planck's constant. $\Delta S^{\ddagger}$ and $\Delta H^{\ddagger}$ are the difference between the initial and transition states for enthalpy and entropy, respectively. The change in enthalpy ($\Delta H^{\ddagger}$) was replaced with the change in energy ($\Delta E^{\ddagger}$) as the volume change is negligible in the reaction. The entropies for the gas phase molecules were calculated from the translational, rotational, and vibrational partition functions. For adsorbed molecules, only the vibrational partition function was used. Thus, the translations and rotations were described as frustrated vibrations. The vibrational modes were evaluated in the harmonic approximation.[6] The NO turnover frequency (TOF) was calculated by summing the elementary steps that consume NO and is reported per Cu-ion per second.

Results and discussion

Experiments

The effect of hydrothermal aging on the activity and selectivity is measured for a 3.2 wt% Cu-CHA sample with an SAR of 13.4. The dependence of the reaction rate constant on the aging duration is shown in Fig. 2. A sharp drop in activity is observed during the first 2 hours. The rate constant decreases from 39 to 11 mol g^{-1} h^{-1}. Thus, the catalyst shows a fast initial deactivation. Beyond 2 hours of aging, the rate constant decreases gradually, indicating a slower rate of deactivation.

The hydrothermal aging also affects the selectivity to N_2O. During the first 10 h of aging, the N_2O selectivity increases from 0.1% to 0.7%. According to the kinetic model,[6] an increase in N_2O selectivity is consistent with a loss of Brønsted acid sites, as the presence of Brønsted acid sites affects the decomposition of the HONO and H_2NNO intermediates to N_2 and H_2O. In the absence of Brønsted acid sites close to species C in Fig. 1, H_2NNO can decompose over species C to form N_2O.

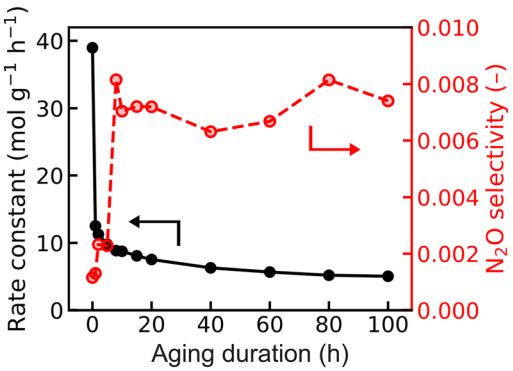

Fig. 2 Rate constants (mol g^{-1} h^{-1}) for NO conversion and N_2O selectivity as a function of hydrothermal aging duration at 650 °C for 3.2 wt% Cu-CHA (an SAR of 13.4). Measurements were performed using 50 mg of catalyst exposed to a gas mixture containing 500 ppm NO, 600 ppm NH_3, 10% O_2, and 5% H_2O, at 160 °C in an N_2 carrier gas with a total flow rate of 13.5 NL h^{-1}.

To directly measure how hydrothermal aging duration affects the amount of Brønsted acid sites, NH_3-TPD measurements are performed on H-CHA and 3.2 wt% Cu-CHA. H-CHA contains Brønsted acid sites and is included as a reference. The fresh H-CHA sample exhibits a single, high-intensity desorption peak centered at approximately 420 °C (Fig. 3(a)). The intensity at 420 °C decreases rapidly during the first 10 hours of hydrothermal aging, and a new peak at around 250 °C appears. Further aging leads to a limited decrease in the amount of adsorbed ammonia in the range of 200–500 °C. The low-temperature NH_3 desorption feature at 250 °C can be associated with NH_3 desorbing from Si–OH/Al–OH formed during dealumintaion,[53] whereas the peak at 420 °C corresponds to NH_3 release from Brønsted acid sites.[27,54] Assuming that all Brønsted acid sites have been lost after 100 h of aging, these data are used as a baseline reference for the quantification of Brønsted acid sites. The quantification is done by integrating the baseline-corrected NH_3–TPD profiles. The Brønsted acid site concentration for the fresh sample is determined to be 1229 μmol g^{-1}. After hydrothermal aging at 650 °C for 2 hours, a sharp decrease in peak intensity is observed. After 2 hours of aging, the Brønsted acid site concentration is 265 μmol g^{-1} and decrease further to 129 μmol g^{-1} after 10 hours of aging. This shows that most Brønsted acid sites are lost within the first 2 hours of aging as a result of dealumination.

In addition to H-CHA, NH_3 TPD was also performed on 3.2 wt% Cu-CHA (an SAR of 13.4), as shown in Fig. 3(b). The fresh Cu-CHA sample exhibits two distinct NH_3 desorption peaks centered at approximately 250 and 420 °C, respectively. The low-temperature peak (250 °C) corresponds to NH_3 release from Lewis acid sites, *e.g.* Cu-sites, whereas the high temperature peak (420 °C) again is attributed to Brønsted acid sites.[27,54] Upon aging, the peak at 280 °C increases and shifts to lower temperatures, whereas the intensity for the peak at 420 °C decreases. The most significant changes are observed during the first 10 hours of aging. The amount of Brønsted acid sites was in this case quantified by a three-peak deconvolution, fixing the high-temperature peak related to the Brønsted acid sites between 395 and 415 °C and allowing the temperatures for the two other peaks to shift during the fitting procedure. This procedure is simplistic with the purpose of performing a semi-quantitative measurement of the loss of Brønsted acid sites. The Brønsted acid site concentration is analyzed to be 930 μmol g^{-1} for the fresh sample. The concentration after 2, 10 and 100 hours of aging is reduced to 426, 241 and 115 μmol g^{-1}, respectively. For Cu-CHA, the decrease in Brønsted acid sites, in addition to dealumination, could arise from the transformation of ZCuOH to Z_2Cu during dealumination.[27]

In addition to the loss of Brønsted acid sites as a result of hydrothermal aging, the decrease in activity can also be related to the loss of Cu sites. To evaluate how hydrothermal aging affects the formation of the $[Cu_2(NH_3)_4O_2]^{2+}$ complex,

 This journal is © The Royal Society of Chemistry 2026

Open Access Article. Published on 06 March 2026. Downloaded on 5/11/2026 12:46:31 PM.
This article is licensed under a Creative Commons Attribution 3.0 Unported Licence.

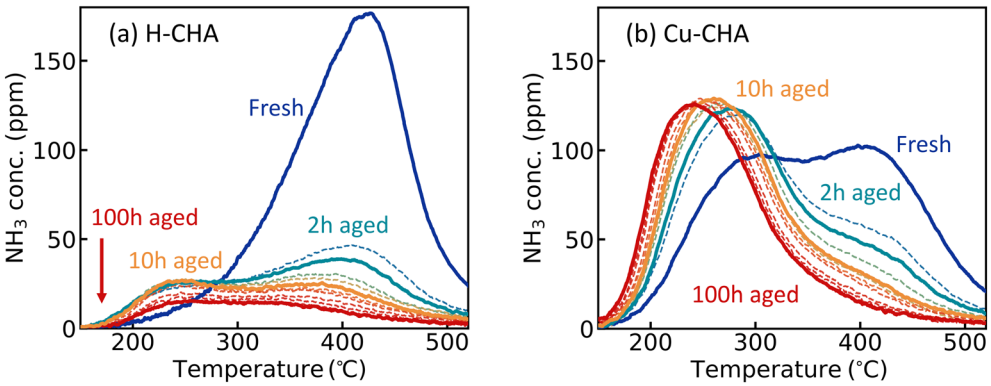

Fig. 3 (a) NH_3 desorption profiles of H-CHA measured after different hydrothermal aging durations (from 0 h to 100 h). (b) NH_3 desorption profiles of 3.2 wt% Cu-CHA (an SAR of 13.4) for different hydrothermal aging durations (from 0 h to 100 h). Dashed lines correspond to intermediate aging stages between fresh and 100 h.

we performed temperature programmed NO reaction experiments for the fresh and aged samples (Fig. 4). A high consumption of NO corresponds to a high amount of $[Cu_2(NH_3)_4O_2]^{2+}$ species. The extent of NO consumption is quantified by integrating the outlet NO concentration curve between 95 °C and 200 °C. Temperatures above 200 °C are excluded, as additional effects unrelated to the NO–$[Cu_2(NH_3)_4O_2]^{2+}$ reaction contribute to the NO consumption at higher temperatures. Moreover, the thermal decomposition of $[Cu_2(NH_3)_4O_2]^{2+}$ starts at about 250 °C.[16,55]

Fig. 4(a) shows the NO outlet concentration profiles after the reaction with $[Cu_2(NH_3)_4O_2]^{2+}$. In all cases, a pronounced decrease in NO concentration is observed between 70 °C and 130 °C, with a minimum near 120–135 °C. The experiments show that NO reacts with the $[Cu_2(NH_3)_4O_2]^{2+}$ complex. At temperatures above 130 °C, the NO concentration rises and approaches the baseline. The fresh catalyst shows the highest consumption of NO. The NO consumption decreases with aging and the 100 h aged sample shows the lowest amount of consumed NO. The experiments show that hydrothermal aging suppresses the formation of the $[Cu_2(NH_3)_4O_2]^{2+}$ species.

To illustrate the trend with suppressed $[Cu_2(NH_3)_4O_2]^{2+}$ formation, Fig. 4(b) shows the ratio of consumed NO between the fresh and aged catalysts. The ratio decreases to 0.87 after 2 hours and 0.68 after 10 hours. While the NH_3-TPD and N_2O selectivity showed only minor changes between 10 and 100 h aging, the ratio of consumed NO between the fresh and aged catalysts is 0.21 after 100 hours, indicating that the ability to form $[Cu_2(NH_3)_4O_2]^{2+}$ complexes keeps declining after 10 h of aging.

DFT calculations and kinetic modeling

In the reaction mechanism presented in the introduction (Fig. 1), the function of the Brønsted acid sites is to decompose the HONO and H_2NNO intermediates to N_2 and H_2O.[5] The results presented in the previous section show that the Cu-CHA catalyst retains some NH_3-SCR activity after 10 h, even though most Brønsted acid sites are lost. This suggests that the decomposition does not necessarily proceed over a Brønsted acid site, and also could occur over the silanol nests formed upon dealumination of the zeolite framework. As the barrier for H_2NNO decomposition in the gas phase is high (1.45 eV),[21] a proton source is needed to facilitate the decomposition. In the absence of Brønsted acid sites, it is possible that silanol groups formed during dealumination

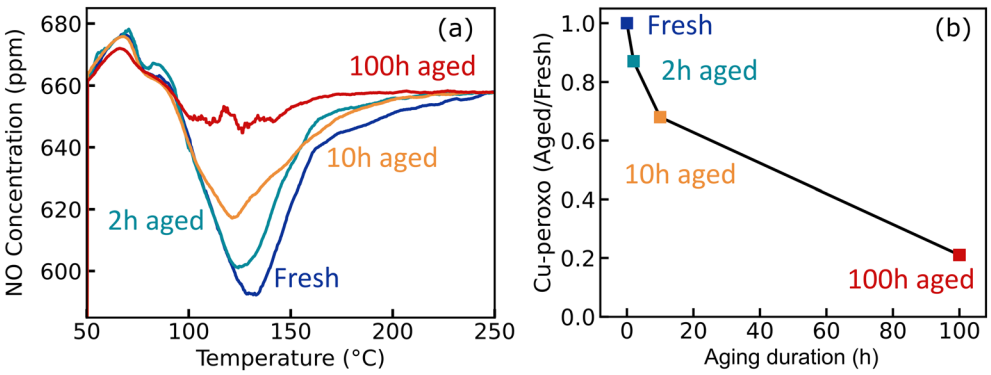

Fig. 4 (a) Temperature-programmed reaction between NO and the $[Cu_2(NH_3)_4O_2]^{2+}$ species comparing the fresh and aged samples (2, 10 and 100 hours). (b) The ratio of consumed NO between the fresh and aged catalysts.

Open Access Article. Published on 06 March 2026. Downloaded on 5/11/2026 12:46:31 PM.
This article is licensed under a Creative Commons Attribution 3.0 Unported Licence.

can act as proton sources. To explore this hypothesis, we performed density functional theory (DFT) calculations of HONO and H_2NNO decomposition over silanol groups.

Fig. 5 shows the potential energy landscape for the decomposition of HONO over a silanol nest (four Si–OH groups). In the first step of the reaction, NH_3 is coordinating to HONO, forming HONO–NH_3. A proton transfer from NH_3 to HONO with simultaneous cleavage of the HO–NO bond results in the formation of H_2NNO and an H_2O molecule. This step has a barrier of 0.42 eV. The H_2NNO intermediate decomposes further to N_2 and another H_2O molecule. The overall reaction is exothermic by −0.76 eV. The mechanism for HONO decomposition over a silanol group differs from that over a Brønsted acid site as the silanol group facilitates a direct proton transfer from NH_3 to HONO with simultaneous HO–NO bond cleavage, forming H_2NNO and H_2O. In the HONO decomposition over a Brønsted site, HONO reacts with the proton forming an NH_3–NO^+ intermediate and H_2O, followed by proton transfer from NH_3–NO^+ to NH_3, which yields H_2NNO and NH_4^+.

Fig. 6 shows the reaction pathway for the decomposition of H_2NNO over a silanol nest. The reaction begins with the adsorption of H_2NNO onto the hydroxyl (OH) group of the silanol nest, forming structure I. Subsequently, a proton is transferred between the OH-group and the adsorbed H_2NNO, leading to the formation of an HNNOH intermediate (structure II). The proton transfer is associated with a barrier of 0.31 eV. The nitrogen atom of HNNOH forms a hydrogen bond with the silanol group (structure II). Next, the OH group of HNNOH rotates, resulting in *trans–trans* HNNOH (structure III) first and thereafter *trans–cis* HNNOH (structure IV). The rotations are associated with barriers of 0.59 and 0.45 eV, respectively. The *trans–cis* HNNOH structure decomposes without a barrier to N_2 and H_2O. The overall reaction is exothermic by −2.45 eV. The H_2NNO decomposition over NH_4^+, which is the state of the Brønsted acid site under reaction conditions, in ref. 5 was proposed to involve multiple proton exchanges, whereas the

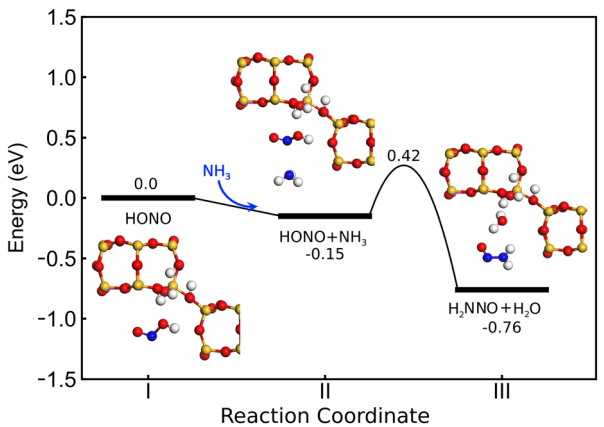

Fig. 5 The potential energy landscape for HONO decomposition over a silanol nest. Atomic color codes: N (blue), O (red), Si (yellow), and H (white).

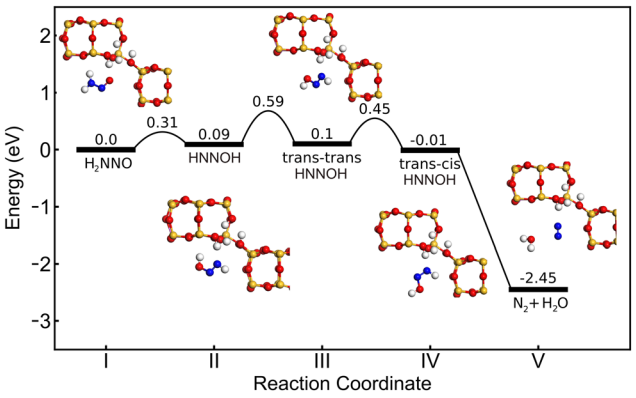

Fig. 6 The potential energy landscape for H_2NNO decomposition over a silanol nest. Atomic color codes: N (blue), O (red), Si (yellow), and H (white).

decomposition over a silanol group proceeds *via* a single proton transfer followed by OH rotations.

The calculations show that the decomposition of HONO and H_2NNO can also occur over the silanol group. However, the highest barrier for decomposition over silanol groups is 0.59 eV, which is higher than the corresponding value (0.38 eV) for decomposition over NH_4^+. Thus, HONO and H_2NNO can decompose over silanol groups if Brønsted acid sites are removed, however, at a slower rate.

To explore the kinetic consequences when exchanging Brønsted acid sites with silanol groups, we calculated the rate of the entire NH_3-SCR cycle using DFT-based microkinetic modeling. The modified model is an extension our previous model.[6,7] Fig. 7 shows the turnover frequency (TOF) as a function of temperature for two cases: i) NH_3-SCR with HONO and H_2NNO decomposition over Brønsted acid sites (solid line) and ii) NH_3-SCR with HONO and H_2NNO decomposition over silanol nests (dashed line). In both cases, the light-off is at about 150 °C and reaches a maximum at 280 °C. The decrease in TOF at higher temperatures is related to a low coverage of adsorbed O_2.[6] The TOF for the NH_3-SCR reaction is lower over silanol groups, as compared to Brønsted acid sites. At 160 °C, the TOF over Brønsted acid

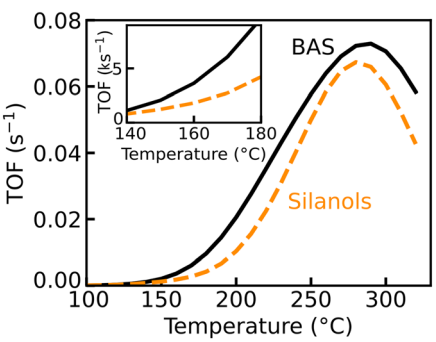

Fig. 7 Simulated turnover frequencies for NO conversion over Cu-CHA as a function of temperature over Brønsted acid sites (solid black line) and silanol groups (dashed orange line). The inset shows a close up of the TOFs around 160 °C.

This journal is © The Royal Society of Chemistry 2026

Open Access Article. Published on 06 March 2026. Downloaded on 5/11/2026 12:46:31 PM. This article is licensed under a Creative Commons Attribution 3.0 Unported Licence.

sites is 0.0038 s^{-1}, whereas it is 0.0018 s^{-1} over the silanol nests. Thus, the TOF is reduced by 50% when the site for HONO and H_2NNO decomposition is changed. The reduced TOF is associated with a change in rate controlling steps as revealed by a degree of rate control analysis[56,57] (see SI). In the case of HONO and H_2NNO decomposition over Brønsted acid sites, the rate is controlled by the blocking of the $[Cu_2(NH_3)_4O_2]^{2+}$ peroxo complex, which hinders NO adsorption and NO reacting with the $[Cu_2(NH_3)_4(OH)_2]^{2+}$ complex. In the case of HONO and H_2NNO decomposition over silanol nests, the rate controlling steps are the NH_3 blocking of the $[Cu_2(NH_3)_4O_2]^{2+}$ peroxo and H_2NNO decomposition.

The higher barrier for HONO and H_2NNO decomposition also affects the selectivity to N_2O. The increased barrier for H_2NNO decomposition results in a higher H_2NNO coverage on the $[Cu_2(NH_3)_4OOH]^{2+}$ intermediate where it decomposes to N_2O and H_2O forming $[Cu_2(NH_3)_4OH]^{2+}$. The selectivity to N_2O is according to the model increased by a factor of 10 at 160 °C, which is in accordance with the experiments in Fig. 2.

To compare the calculated rates for the NH_3-SCR reaction with the measurements, there is a need to account for the loss of Cu sites. The NO-TPR experiments show that 13%, 32% and 79% of the $[Cu_2(NH_3)_4O_2]^{2+}$ complexes relative to the fresh sample are lost after 2, 10 and 100 hours of aging, respectively. The loss of $[Cu_2(NH_3)_4O_2]^{2+}$ complexes can be assumed to be related to a reduced formation of $Cu(NH_3)_2^+$ pairs. Because the starting point in the kinetic model is a pair of $Cu(NH_3)_2^+$ complexes, the reduced number of $[Cu_2(NH_3)_4O_2]^{2+}$ complexes is accounted for by simply reducing the number of paired $Cu(NH_3)_2^+$ complexes in the model.

Combining the effects of HONO and H_2NNO decomposition over silanol groups and the loss of $Cu(NH_3)_2^+$ pairs results in a reduction of the TOF by 56%, 66% and 94% as compared to the case with HONO and H_2NNO decomposition over Brønsted acid sites and the initial number of $Cu(NH_3)_2^+$ pairs. Experimentally, the corresponding decreases in the rate constant with respect to the fresh sample are 72%, 78% and 89% for the samples aged for 2, 10 and 100 hours, respectively (Fig. 2). The simulated rates show a similar trend to the measured deactivation, indicating that the initial rapid deactivation is associated with the loss of Brønsted acid sites, whereas the slow deactivation arises from the decrease in available $Cu(NH_3)_2^+$ complexes.

Discussion

The NH_3-SCR activity measurements of Cu-CHA indicate two kinds of deactivation mechanisms with different rate constants upon hydrothermal aging. A fast deactivation occurs within the first 10 hours of aging followed by a slower deactivation mechanism from 10 to 100 hours of aging. The initial fast decrease in the activity coincides with a rapid loss of Brønsted acid sites and an increase in N_2O selectivity, which remains largely constant after 10 h aging. The observation that the catalyst still shows activity after hydrothermal aging suggests that the HONO and H_2NNO decomposition occurs over silanol nests that are formed upon dealumination, however, at a lower rate than that over the Brønsted acid sites. The experimental finding is supported by DFT calculations, showing that HONO and H_2NNO decompose over silanol groups with a barrier that is higher than that over Brønsted acid sites (0.59 eV as compared to 0.38 eV).

Dealumination also affects the mobility and pairing of $Cu(NH_3)_2^+$ complexes. A pair of $Cu(NH_3)_2^+$ complexes is required for O_2 adsorption and the formation of the $[Cu_2(NH_3)_4O_2]^{2+}$ complex. The NO-TPR experiments show that the amount of $[Cu_2(NH_3)_4O_2]^{2+}$ complexes is reduced to 68% after 10 hours of aging and to 21% after 100 hours of aging. The reduced amount of formed $[Cu(NH_3)_4O_2]^{2+}$ complexes could, for example, originate from i) reduced mobility of $Cu(NH_3)_2^+$ complexes, ii) lower stability of paired $Cu(NH_3)_2^+$ complexes and $[Cu_2(NH_3)_4O_2]^{2+}$, and iii) the formation of Cu-aluminate species, which are inactive for NH_3-SCR. The experiments indicate that once the majority of Brønsted acid sites are lost, the rate becomes increasingly controlled by the formation of $[Cu_2(NH_3)_4O_2]^{2+}$ complexes, which are key intermediates in the NH_3-SCR cycle.

The hydrothermal aging is also investigated with a DFT-based microkinetic model, incorporating the effect of replacing Brønsted acid sites with silanol groups and a reduced number of paired $Cu(NH_3)_2^+$ complexes. Including only the effect of HONO and H_2NNO decomposition of silanol groups results in a 50% decrease in the TOF at 160 °C as compared to the pristine case. Adding the effects of a reduced number of paired $Cu(NH_3)_2^+$ complexes results in a reduction of the TOF that is close to the reduction of the experimental values of the rate constant. It should be noted that the onset of the NH_3-SCR reaction is controlled by desorption of NH_3 from $[Cu_2(NH_3)_5O_2]^{2+}$, which enables NO adsorption and subsequently NO–NH_3 coupling.[6]

Although the current micro-kinetic model is in line with the experiments, there are important limitations. The model does not account for changes in the Al-distribution upon dealumination. The change in Al-distribution affects the stability of the paired $Cu(NH_3)_2^+$ complexes as well as the adsorption energies of O_2, NO and NH_3.[36] Moreover, the model does not account for changes in diffusion barriers of H_2NNO and HONO, which affects the selectivity to N_2O.

Conclusions

We have combined activity measurements, NH_3-temperature programmed desorption, NO-temperature programmed reaction, and DFT-based microkinetic modeling to investigate the hydrothermal aging of Cu-CHA catalysts for NH_3-SCR. The activity measurement revealed two types of deactivation processes, a fast initial process that dominates the first 10 hours of deactivation and a slower process that is active during the rest of the deactivation measurements. The initial

Open Access Article. Published on 06 March 2026. Downloaded on 5/11/2026 12:46:31 PM.
This article is licensed under a Creative Commons Attribution 3.0 Unported Licence.

fast deactivation coincides with a rapid decrease of Brønsted acid sites and an increased selectivity to N_2O. The slower process is connected to the formation of $[Cu_2(NH_3)_4O_2]^{2+}$ complexes.

The experiments have been corroborated by DFT-based kinetic modeling. The model relies on copper sites to form HONO and H_2NNO and Brønsted acid sites or silanol groups for HONO and H_2NNO decomposition to N_2 and H_2O.[6] The model shows that the initial fast decrease in activity can be related to the loss of Brønsted acid sites as the rate for HONO and H_2NNO decomposition is slower on silanol groups than on Brønsted acid sites. Moreover, the slower rate for H_2NNO decomposition results in an increased selectivity to N_2O. The remaining deactivation can be related to the decrease in $[Cu_2(NH_3)_4O_2]^{2+}$ formation as measured in the NO-TPR experiments. This work shows that hydrothermal aging severely affects the performance of the Cu-CHA system for NH_3-SCR and that the loss in performance can be understood within the framework of an atomistic DFT-based kinetic model.

Author contributions

Shivangi Singh: investigation and writing – original draft. Ton V. W. Janssens: supervision, writing – review and editing, and funding acquisition. Henrik Grönbeck: supervision, writing – review and editing, and funding acquisition.

Conflicts of interest

There are no conflicts of interest to declare.

Data availability

Structural data from the DFT calculations are deposited in the Zenodo database under accession code https://doi.org/10.5281/zenodo.18761153.

Supplementary information (SI): kinetic parameters for the elementary steps in the kinetic model; procedure for the quantification of Brønsted acid sites for H-CHA based on TPD experiments; degree of rate control analysis. See DOI: https://doi.org/10.1039/d5cy01491c.

Acknowledgements

We acknowledge the support from the European Union's Horizon 2020 Research and Innovation Programme under the Marie Sklodowska-Curie grant agreement no. 955839 (CHASS). The calculations were performed at PDC (Stockholm) and NSC (Linköping) through a NAISS grant (2022/3-14). The Competence Centre for Catalysis (KCK) is hosted by Chalmers University of Technology and financially supported by the Swedish Energy Agency (52689-1) and the member companies Johnson Matthey, Perstorp, Powercell, Preem, Scania CV, Umicore and Volvo Group.

References

1 *Urea-SCR technology for deNO$_x$ after treatment of diesel exhausts*, ed. I. Nova and E. Tronconi, Springer, 2014, vol. 5.
2 D. W. Fickel, E. D'Addio, J. A. Lauterbach and R. F. Lobo, The ammonia selective catalytic reduction activity of copper-exchanged small-pore zeolites, *Appl. Catal., B*, 2011, **102**, 441–448.
3 S. J. Schmieg, S. H. Oh, C. H. Kim, D. B. Brown, J. H. Lee, C. H. Peden and D. H. Kim, Thermal Durability of Cu-CHA NH_3-SCR Catalysts for Diesel NO_x Reduction, *Catal. Today*, 2012, **184**, 252–261.
4 Y. Xin, Q. Li and Z. Zhang, Zeolitic Materials for DeNO$_x$ Selective Catalytic Reduction, *ChemCatChem*, 2018, **10**, 29–41.
5 L. Chen, T. V. W. Janssens, P. N. R. Vennestrøm, J. Jansson, M. Skoglundh and H. Grönbeck, A complete multisite reaction mechanism for low-temperature NH_3-SCR over Cu-CHA, *ACS Catal.*, 2020, **10**, 5646–5656.
6 Y. Feng, X. Wang, T. V. W. Janssens, P. N. R. Vennestrøm, J. Jansson, M. Skoglundh and H. Grönbeck, First-Principles Microkinetic Model for Low-Temperature NH_3-Assisted Selective Catalytic Reduction of NO over Cu-CHA, *ACS Catal.*, 2021, **11**, 14395–14407.
7 S. Singh, Y. Feng, T. V. W. Janssens and H. Grönbeck, Inhibition of NH3-SCR over Cu-CHA at high partial pressures of water: Measurements and DFT-based kinetic modeling, *J. Catal.*, 2025, **446**, 116071.
8 C. Paolucci, A. A. Verma, S. A. Bates, V. F. Kispersky, J. T. Miller, R. Gounder, W. N. Delgass, F. H. Ribeiro and W. F. Schneider, Isolation of the Copper Redox Steps in the Standard Selective Catalytic Reduction on Cu-SSZ-13, *Angew. Chem., Int. Ed.*, 2014, **53**, 11828–11833.
9 F. Gao, D. Mei, Y. Wang, J. Szanyi and C. H. Peden, Selective Catalytic Reduction over Cu/SSZ-13: Linking Homo- and Heterogeneous Catalysis, *J. Am. Chem. Soc.*, 2017, **139**, 4935–4942.
10 C. Paolucci, I. Khurana, A. A. Parekh, S. Li, A. J. Shih, H. Li, J. R. Di Iorio, J. D. Albarracin-Caballero, A. Yezerets and J. T. Miller, others Dynamic multinuclear sites formed by mobilized copper ions in NO_x selective catalytic reduction, *Science*, 2017, **357**, 898–903.
11 W. Hu, T. Selleri, F. Gramigni, E. Fenes, K. R. Rout, S. Liu, I. Nova, D. Chen, X. Gao and E. Tronconi, On the redox mechanism of low-temperature NH3-SCR over Cu-CHA: a combined experimental and theoretical study of the reduction half cycle, *Angew. Chem., Int. Ed.*, 2021, **60**, 7197–7204.
12 C. Liu, S. Yasumura, T. Toyao, Z. Maeno and K.-I. Shimizu, Mechanism of standard NH_3–SCR over Cu-CHA via NO^+ and HONO intermediates, *J. Phys. Chem. C*, 2022, **126**, 11594–11601.
13 J. Abdul Nasir, J. Guan, T. W. Keal, A. W. Desmoutier, Y. Lu, A. M. Beale, C. R. A. Catlow and A. A. Sokol, Influence of solvent on selective catalytic reduction of nitrogen oxides with ammonia over Cu-CHA zeolite, *J. Am. Chem. Soc.*, 2022, **145**, 247–259.

 This journal is © The Royal Society of Chemistry 2026

Open Access Article. Published on 06 March 2026. Downloaded on 5/11/2026 12:46:31 PM. This article is licensed under a Creative Commons Attribution 3.0 Unported Licence.

14 F. Giordanino, E. Borfecchia, K. A. Lomachenko, A. Lazzarini, G. Agostini, E. Gallo, A. V. Soldatov, P. Beato, S. Bordiga and C. Lamberti, Interaction of NH_3 with Cu-SSZ-13 catalyst: a complementary FTIR, XANES, and XES study, *J. Phys. Chem. Lett.*, 2014, **5**, 1552–1559.

15 T. V. W. Janssens, H. Falsig, L. F. Lundegaard, P. N. R. Vennestrøm, S. B. Rasmussen, P. G. Moses, F. Giordanino, E. Borfecchia, K. A. Lomachenko, C. Lamberti, S. Bordiga, A. Godiksen, S. Mossin and P. Beato, A consistent reaction scheme for the selective catalytic reduction of nitrogen oxides with ammonia, *ACS Catal.*, 2015, **5**, 2832–2845.

16 K. A. Lomachenko, E. Borfecchia, C. Negri, G. Berlier, C. Lamberti, P. Beato, H. Falsig and S. Bordiga, The Cu-CHA deNO_x catalyst in action: temperature-dependent NH_3-assisted selective catalytic reduction monitored by operando XAS and XES, *J. Am. Chem. Soc.*, 2016, **138**, 12025–12028.

17 L. Chen, J. Jansson, M. Skoglundh and H. Grönbeck, Mechanism for solid-state ion exchange of Cu^+ into zeolites, *J. Phys. Chem. C*, 2016, **120**, 29182–29189.

18 C. Paolucci, I. Khurana, A. A. Parekh, S. Li, A. J. Shih, H. Li, J. R. Di Iorio, J. D. Albarracin-Caballero, W. F. Schneider and R. Gounder, Dynamic Multinuclear Sites Formed by Mobilized Copper Ions in NO_x Selective Catalytic Reduction, *Science*, 2017, **357**, 898–903.

19 L. Chen, H. Falsig, T. V. W. Janssens and H. Grönbeck, Activation of oxygen on $(NH_3–Cu–NH_3)^+$ in NH_3-SCR over Cu-CHA, *J. Catal.*, 2018, **358**, 179–186.

20 T. V. W. Janssens, E. Borfecchia, K. A. Lomachenko, H. Grönbeck and G. Berlier, The $[(NH_3)_4Cu_2O_2]^{2+}$-Peroxo Complex as the Key Intermediate for NH_3-SCR Activity and Deactivation of Cu-CHA Catalysts, *ChemCatChem*, 2024, **16**, e202400384.

21 L. Chen, T. V. W. Janssens, P. N. R. Vennestrom, J. Jansson, M. Skoglundh and H. Grönbeck, A Complete Multisite Reaction Mechanism for Low-Temperature NH_3-SCR over Cu-CHA, *ACS Catal.*, 2020, **10**, 5646–5656.

22 Y. Feng, T. V. W. Janssens, P. N. R. Vennestrøm, J. Jansson, M. Skoglundh and H. Grönbeck, The role of H^+-and Cu^+-sites for N_2O formation during NH_3-SCR over Cu-CHA, *J. Phys. Chem. C*, 2021, **125**, 4595–4601.

23 S. M. Campbell, D. M. Bibby, J. M. Coddington, R. F. Howe and R. H. Meinhold, Dealumination of HZSM-5 zeolites: I. Calcination and hydrothermal treatment, *J. Catal.*, 1996, **161**, 338–349.

24 T. Masuda, Y. Fujikata, S. R. Mukai and K. Hashimoto, Changes in catalytic activity of MFI-type zeolites caused by dealumination in a steam atmosphere, *Appl. Catal., A*, 1998, **172**, 73–83.

25 S. Malola, S. Svelle, F. L. Bleken and O. Swang, Detailed reaction paths for zeolite dealumination and desilication from density functional calculations, *Angew. Chem., Int. Ed.*, 2012, **51**, 652–655.

26 M.-C. Silaghi, C. Chizallet, J. Sauer and P. Raybaud, Dealumination mechanisms of zeolites and extra-framework aluminum confinement, *J. Catal.*, 2016, **339**, 242–255.

27 J. Luo, F. Gao, K. Kamasamudram, N. Currier, C. H. Peden and A. Yezerets, New insights into Cu/SSZ-13 SCR catalyst acidity. Part I: Nature of acidic sites probed by NH_3 titration, *J. Catal.*, 2017, **348**, 291–299.

28 F. Gao and J. Szanyi, On the hydrothermal stability of Cu/SSZ-13 SCR catalysts, *Appl. Catal., A*, 2018, **560**, 185–194.

29 M. Wenig, R. Khare, A. Jentys and J. A. Lercher, Hydrothermal Stability of Active Sites in Cu-Exchanged Small-Pore Zeolites for the Selective Catalytic Reduction of NO_x, *Angew. Chem., Int. Ed.*, 2025, **64**, e202416954.

30 P. N. R. Vennestrøm, T. V. W. Janssens, A. Kustov, M. Grill, A. Puig-Molina, L. F. Lundegaard, R. R. Tiruvalam, P. Concepción and A. Corma, Influence of lattice stability on hydrothermal deactivation of Cu-ZSM-5 and Cu-IM-5 zeolites for selective catalytic reduction of NO_x by NH_3, *J. Catal.*, 2014, **309**, 477–490.

31 J. D. Albarracin-Caballero, I. Khurana, J. R. Di Iorio, A. J. Shih, J. E. Schmidt, M. Dusselier, M. E. Davis, A. Yezerets, J. T. Miller and F. H. Ribeiro, others Structural and kinetic changes to small-pore Cu-zeolites after hydrothermal aging treatments and selective catalytic reduction of NO_x with ammonia, *React. Chem. Eng.*, 2017, **2**, 168–179.

32 S. Singh, T. V. W. Janssens and H. Grönbeck, Mechanism for Cu-enhanced hydrothermal stability of Cu–CHA for NH_3-SCR, *Catal. Sci. Technol.*, 2024, **14**, 3407–3415.

33 J. C. Navarro de Miguel, S.-H. Chung, A. Dikhtiarenko, T. Li, J. Patarroyo and J. Ruiz-Martinez, Brønsted acid-site density controls the mechanistic cycle and product selectivity in the methanol-to-hydrocarbons reaction in BEA zeolite, *ACS Catal.*, 2024, **14**, 5989–6000.

34 Y. Fu, W. Ding, H. Lei, Y. Sun, J. Du, Y. Yu, U. Simon, P. Chen, Y. Shan and G. He, others Spatial Distribution of Brønsted Acid Sites Determines the Mobility of Reactive Cu Ions in the Cu-SSZ-13 Catalyst during the Selective Catalytic Reduction of NO_x with NH_3, *J. Am. Chem. Soc.*, 2024, **146**, 11141–11151.

35 J. D. Bjerregaard, M. Votsmeier and H. Grönbeck, Influence of aluminium distribution on the diffusion mechanisms and pairing of $[Cu(NH_3)_2]^+$ complexes in Cu-CHA, *Nat. Commun.*, 2025, **16**, 603.

36 Y. Feng and H. Grönbeck, Kinetic Monte Carlo Simulations of Low-Temperature NH_3-SCR over Cu-Exchanged Chabazite, *ChemPhysChem*, 2024, **25**, e202400558.

37 N. D. Nasello, N. Usberti, U. Iacobone, F. Gramigni, W. Hu, S. Liu, I. Nova, X. Gao and E. Tronconi, Dual-Site RHC and OHC transient kinetics predict low-T standard SCR steady-state rates over a Cu-CHA catalyst, *ACS Catal.*, 2023, **13**, 2723–2734.

38 W. P. Partridge, S. Y. Joshi, J. A. Pihl and N. W. Currier, New operando method for quantifying the relative half-cycle rates of the NO SCR redox cycle over Cu-exchanged zeolites, *Appl. Catal., B*, 2018, **236**, 195–204.

39 F. Gao, E. D. Walter, E. M. Karp, J. Luo, R. G. Tonkyn, J. H. Kwak, J. Szanyi and C. H. Peden, Structure–activity relationships in NH_3-SCR over Cu-SSZ-13 as probed by reaction kinetics and EPR studies, *J. Catal.*, 2013, **300**, 20–29.

Open Access Article. Published on 06 March 2026. Downloaded on 5/11/2026 12:46:31 PM.
This article is licensed under a Creative Commons Attribution 3.0 Unported Licence.

40 A. Y. Molokova, D. Salusso, E. Borfecchia, F. Wen, S. Magliocco, S. Bordiga, T. V. W. Janssens, K. A. Lomachenko and G. Berlier, The chemical nature of SO_2 poisoning of Cu-CHA-based SCR catalysts for NO_x removal in diesel exhausts, *Catal. Sci. Technol.*, 2024, **14**, 5989–5995.
41 C. Negri, T. Selleri, E. Borfecchia, A. Martini, K. A. Lomachenko, T. V. Janssens, M. Cutini, S. Bordiga and G. Berlier, Structure and reactivity of oxygen-bridged diamino dicopper(II) complexes in Cu-ion-exchanged chabazite catalyst for NH_3-mediated selective catalytic reduction, *J. Am. Chem. Soc.*, 2020, **142**, 15884–15896.
42 A. Y. Molokova, E. Borfecchia, A. Martini, I. A. Pankin, C. Atzori, O. Mathon, S. Bordiga, F. Wen, P. N. R. Vennestrom and G. Berlier, others SO_2 Poisoning of Cu-CHA deNO_x Catalyst: The Most Vulnerable Cu Species Identified by X-ray Absorption Spectroscopy, *JACS Au*, 2022, **2**, 787–792.
43 G. Kresse and J. Hafner, Ab Initio Molecular Dynamics for Open-Shell Transition Metals, *Phys. Rev. B: Condens. Matter Mater. Phys.*, 1993, **48**, 13115–13118.
44 G. Kresse and J. Hafner, Ab Initio Molecular-Dynamics Simulation of the Liquid-Metalamorphous-Semiconductor Transition in Germanium, *Phys. Rev. B: Condens. Matter Mater. Phys.*, 1994, **49**, 14251–14269.
45 G. Kresse and J. Furthmüller, Efficient Iterative Schemes for Ab Initio Total-Energy Calculations Using a Plane-Wave Basis Set, *Phys. Rev. B: Condens. Matter Mater. Phys.*, 1996, **54**, 11169–11186.
46 G. Kresse and J. Furthmüller, Efficiency of Ab-Initio Total Energy Calculations for Metals and Semiconductors using a Plane-Wave Basis Set, *Comput. Mater. Sci.*, 1996, **6**, 15–50.
47 P. E. Blöchl, Projector Augmented-Wave Method, *Phys. Rev. B: Condens. Matter Mater. Phys.*, 1994, **50**, 17953–17979.
48 G. Kresse and D. Joubert, From Ultrasoft Pseudopotentials to the Projector Augmented-Wave Method, *Phys. Rev. B: Condens. Matter Mater. Phys.*, 1999, **59**, 1758–1775.
49 J. P. Perdew, K. Burke and M. Ernzerhof, Generalized Gradient Approximation Made Simple, *Phys. Rev. Lett.*, 1996, **77**, 3865–3868.
50 S. Grimme, J. Antony, S. Ehrlich and H. Krieg, A Consistent and Accurate Ab Initio Parametrization of Density Functional Dispersion Correction (DFT-D) for the 94 Elements H-Pu, *J. Chem. Phys.*, 2010, **132**, 154104.
51 S. Grimme, S. Ehrlich and L. Goerigk, Effect of the Damping Function in Dispersion Corrected Density Functional Theory, *J. Comput. Chem.*, 2012, **32**, 1456–1465.
52 I. Chorkendorff and J. W. Niemantsverdriet, *Concepts of Modern Catalysis and Kinetics*, John Wiley & Sons, 2017, p. 109.
53 S. A. Skarlis, D. Berthout, A. Nicolle, C. Dujardin and P. Granger, Multisite modeling of NH_3 adsorption and desorption over Fe-ZSM5, *J. Phys. Chem. C*, 2012, **116**, 8437–8448.
54 S. A. Bates, W. N. Delgass, F. H. Ribeiro, J. T. Miller and R. Gounder, Methods for NH_3 titration of Brønsted acid sites in Cu-zeolites that catalyze the selective catalytic reduction of NO_x with NH_3, *J. Catal.*, 2014, **312**, 26–36.
55 E. Borfecchia, C. Negri, K. A. Lomachenko, C. Lamberti, T. V. W. Janssens and G. Berlier, Temperature-dependent dynamics of NH_3-derived Cu species in the Cu-CHA SCR catalyst, *React. Chem. Eng.*, 2019, **4**, 1067–1080.
56 C. T. Campbell, Future Directions and Industrial Perspectives Micro- and Macro-Kinetics: Their Relationship in Heterogeneous Catalysis, *Top. Catal.*, 1994, **1**, 353–366.
57 C. T. Campbell, The degree of rate control: A powerful tool for catalysis research, *ACS Catal.*, 2017, **7**, 2770–2779.

 This journal is © The Royal Society of Chemistry 2026